NEAR WALL FLOW STRUCTURE OF INCLINED CYLINDER INTERACTING WITH DIFFERENT BOUNDARY LAYER THICKNESS

Takaaki Shizawa
Department of Mechanical Engineering, Science University of Tokyo
1-3 Kagurazaka Shinjuku-ku, Tokyo 1628601, Japan
shizawa@rs.kagu.sut.ac.jp

Kenichi Ohta
Department of Mechanical Engineering, Science University of Tokyo
1-3 Kagurazaka Shinjuku-ku, Tokyo 1628601, Japan
j4599614@ed.kagu.sut.ac.jp

ABSTRACT

A circular cylinder, established on a wall, includes several complex problems in the structure of the flow field. First problem is the spanwise fluctuation of wake shedding and second one is the inclined angle of the cylinder. Next problem is the end effects of the cylinder. Last problem is the turbulence of the approaching free stream.

There is little fundamental research work about the formation and the development of the wake of an inclined cylinder interacting with a boundary layer. This paper presents an experimental study focused on the near wall three-dimensional structure of the inclined cylinder interacting with two cases of boundary layer thickness. A cylinder is established on a flat wall where a two-dimensional turbulent boundary layer is developed. Nine cases of inclined cylinder, inclined angle of ±30°, ±20°, ±15°, ±10° and 0° are investigated. The size of horseshoe vortex is changed exponentially to the inclined angle. The remarkable influences depending on the boundary layer thickness are observed at the structure of the wake, in case of inclined backward and normal cylinder. The structure is not affected by the boundary layer thickness, in case of inclined forward cylinder.

INTRODUCTION

A number of investigators have been concerned with the problems of the formation and the development of three-dimensional structure in turbulent shear flow. One of the research works is the flow around a bluff body, and a cylinder is commonly used as a base case. The wake is three-dimensional even at low Reynolds number. Furthermore, the shedding frequency in a wake is affected by the end conditions of the cylinder.

The circular cylinder includes several complex problems in the structure of the flow field. First problem is the spanwize fluctuation of wake structure, and the wake promotes three-dimensionality of the flow field even at normal cylinder. Second problem is the inclined angle of the cylinder. The inclined angle, even it is small, also promotes three-dimensionality of the wake structure. Next problem is the end effects of the cylinder. Many is the case that the wake of cylinder interacts with the boundary layer. The near wall structure of the wake is changed and the shedding frequency becomes oblique. Last problem is the turbulence of the approaching freestream.

The research works about the cylinder are classified into following four. First one is the research about Karman vortex. Next is the study about inclined angle of the cylinder, and the third is the horseshoe vortex upstream of the cylinder. The last one is the end effects of the cylinder.

Gerrard (1966) reported about the formation region of a Karman vortex in the wake. Humphreys (1960) presented the spanwize change of flow field close to the cylinder. The structure of the wake far downstream of the cylinder was reported by Cimbala et al. (1988). The characteristics of Karman vortex based on the Strouhal number at very low Reynold number were reported by Williamson (1989), the transition region were by Humphreys (1960) and the critical Reynolds number region were by Bearman (1969).

The effects of inclined angle on the Strouhal number of circular cylinder were reported by Hanson (1966), Van Atta, (1968), Smith et al. (1972) and Mangalam et al (1994). Shizawa et al. (1998) reported that the twin type of vortex was observed in the wake, in case of inclined backward cylinder.

Eckerle and Langston (1987) presented a new aspect of the formation of horseshoe vortex. Then, Eckerle and Awad (1991) show that the type of vortex formation was classified into two and proposed the flow parameter.

Gerich and Eckelmann (1982), Eibeck (1990) and Stansby (1974) reported the end effects of cylinder

on the shedding frequency and the wake structure. Ramberg (1983) concluded that the end condition affects very sensitive to the formation of the vortex shedding.

There is only a few information about the formation and the development of the wake of an inclined cylinder interacting with the boundary layer. Then, this paper presents an experimental study focused on the complex three-dimensional structure in turbulent boundary layer. This results present the useful information to understand the structure of the wake under the influence of inclined angle of the cylinder interacting with two cases of the boundary layer thickness.

EXPERIMENTAL SETUP AND METHOD

An inclined cylinder is established on the center of the wind tunnel where a two-dimensional turbulent boundary layer (*BL*) is developed. The test tunnel has 700 mm x 230 mm cross section and 3040 mm in length, as shown in Figure 1. A tripping wire of ϕ1.2 mm in diameter is installed at the outlet straight part of two-dimensional contraction nozzle. The cylinder is installed carefully into the wind tunnel with zero-pitch angle to the approaching freestream. The blockage factor of the cylinder diameter to the wind tunnel width is 4.3 %. Then, the effect of side walls on the structure of the cylinder wake is negligible. The surface roughness of each cylinder is less than 2 μm to minimize the effects of roughness on the separation line of the cylinder surface.

The circular cylinder has D = 30 mm in diameter and covers the whole height of the tunnel. The aspect ratio of the tunnel height to the cylinder diameter is 7.7. Nine cases of inclined cylinder, inclined angle of θ = ±30°, ±20°, ±15°, ±10° and 0° to the free stream, are investigated. The experimental conditions are obtained by changing the established distance of the cylinder from the outlet of the nozzle. In case of "thin *BL*", the cylinder is established on the *BL* thickness of about 60 % of the cylinder diameter. In case of "thick *BL*", the *BL* thickness is about 130 % of the cylinder diameter. The *BL* parameters are listed in Table 1. All the measurements are conducted over the lower wall. Then, the cylinder is merged in the same *BL* thickness. The negative angle corresponds to an inclined forward cylinder (*IFC*), and the positive angle corresponds to an inclined backward cylinder (*IBC*), respectively.

The coordinate system employed is also shown in Figure 1. The origin of streamwise X-direction is the center of the cylinder and Y-direction is the normal distance from the wall. Spectrum of streamwise turbulence intensity is measured at X = 90 mm (X/D = 3). The reference velocity U_r at the reference location X' = 360 mm (X' : distance from the outlet of contraction nozzle) is 13.0 m/s (±1.0 %) and the turbulence intensity is 0.2 %.

An oil film flow visualization technique is used. Wall static pressure is measured by a displacement micro manometer with an accuracy of 0.01 Pa. Turbulence intensity and spectrum are measured by a normal hot-wire anemometer. Calibration is conducted both before and after the run, and the averaged calibration coefficients are used when the differnce is within 3 %. *FFT* analyzer with 16 bits *A/D* converter is used at spectrum measurements. Data is sampled at 12.8 kHz through 7.8 kHz digital low-pass filter and 256 samples are averaged. Uncertainties in measurements, calculated using the method of Kline and Mclintock (1953) are ±3 % for mean flow and ±5 % for turbulence intensity using a hot-wire anemometer and the result is a ±0.3 mm uncertainty for the oil width by an oil film flow visualization.

RESULTS AND DISCUSSIONS

Centerline Wall Static Pressure

Figure 2 and Figure 3 present the centerline static pressure C_{pw} distribution. Figure (a) is the case at thin *BL*, and Figure (b) is the thick *BL* case, respectively. The axis of ordinate of the Figures is the logarithmic coordinate.

Figure 2 shows the C_{pw} at upstream of the cylinder. The C_{pw} is increased linearly and remarkably increased toward the stagnation value of 1, at very close to the cylinder. The slope of C_{pw} is decreased as the inclined angle is increased, in case of *IFC*. On the other hand, in case of *IBC*, the slope is increased as the inclined angle is increased. The differences between Figure 2(a) and Figure 2(b) are apparently small but each slope of C_{pw} is steeper at thick *BL*. The slope of C_{pw} at upstream of the cylinder presents a strong correlation with the size of horseshoe vortex. The smaller the slope, the larger the size of horseshoe vortex is expected. Then, the size of horseshoe vortex is mainly affected by the inclined angle of the cylinder.

Figure 3 presents the centerline static pressure C_{pw} at downstream of the cylinder. The C_{pw} is changed sign so as to show positive value to fit to the logarithmic coordinate. The C_{pw} shows maximum peak and decreases monotonically to downstream, in case of *IFC* and normal cylinder, as shown in Figure 3(a). On the other hand, the C_{pw} presents the minimum peak following to the maximum peak and is increased monotonically to downstream, in case of *IBC*. Figure 3(b) shows the C_{pw} profile at thick *BL*. The profile shows almost the same as thin *BL* case, in case of *IFC*. In case of *IBC*, each minimum peak value of C_{pw} shows larger compared with thin *BL* case. The dispersions of C_{pw} at X/D = 10 are small at

thick BL. The profile of C_{pw} presents the recovery process and the size of wake region. The slow recovery is expected at thin *BL* and rapid recovery is observed at thick *BL*. The comparatively smaller size of wake region is expected at thick *BL*.

The remarkable differences of downstream change of C_{pw} are observed at normal cylinder, presented by open bold circles. The profile shows almost the same pattern as *IFC* at thin *BL*, and it shows the same as *IBC* at thick *BL*.

Figure 4 presents the slope A_1 of C_{pw} with the change of inclined angle θ of the cylinder. Downstream value of A_1 is represented positive value. Again, the negative angle corresponds to the *IFC* and positive angle corresponds to the *IBC*.

$$C_{pw} = \exp\{A_1(X/D) + A_0\} \quad (1)$$

Where, A_1 is the slope of C_{pw} and A_0 is the location of zero crossing at logarithmic coordinate. The A_1 presents a linear function to the inclined angle θ at upstream of the cylinder.

$$\text{Thin } BL: \quad A_1 = 6.5 \times 10^{-3}\theta + 0.8 \quad (2)$$
$$\text{Thick } BL: \quad A_1 = 7.4 \times 10^{-3}\theta + 1.1 \quad (3)$$

At thick *BL* case, the larger value of A_1 is presented than that at thin *BL* case. As mentioned before, the smaller size of horseshoe vortex is expected at thick *BL*. At downstream of the cylinder, the difference of A_1 by the *BL* thickness is little, in case of *IFC*. On the other hand, A_1 is remarkably increased, in case of *IBC*. The A_1 presents larger value but the profile shows weaker correlation with the inclined angle. Also, the A_1 presents larger value at thick *BL*, in case of normal cylinder.

At upstream of the cylinder, the size of horseshoe vortex is changed exponentially to the inclined angle. The size is about 38 % larger at thin *BL* case, compared with thick *BL* case. At downstream of the cylinder, the structure of the wake is almost the same, independent of the *BL* thickness, in case of *IFC*. In case of *IBC*, the wake is strongly affected by the inclined angle.

Figure 5 shows the peak distance of C_{pw} from the cylinder at downstream of the cylinder. In case of *IBC*, peaks at near and far cylinder are observed almost at the same streamwise distance, in spite of *BL* thickness. The distance is decreased as the increase in inclined angle of the cylinder. In case of *IFC*, the distance of the peaks at far cylinder is changed by the inclined angle. In case of thin *BL*, the smaller the inclined angle, the longer the distance is observed. Furthermore, the peak is not observed at small inclined angle and normal cylinder. On the other hand, these peaks are not observed at thick *BL*. Then, this paper is focused on the flow structure of small inclined angle case, as the basic line.

Wall Flow Pattern

Figure 6(a) presents the wall flow pattern by oil film flow visualization, in case of normal cylinder. The upper photo shows the thin *BL* case and the lower is the thick *BL* case, respectively. At the upstream of the cylinder, both the separation line and the line of low mean wall shear stress are located closer to the cylinder, at thick *BL* case, compared with thin *BL* case. The result confirms that the size of horseshoe vortex is larger at thin *BL* compared with thick *BL*. The size of convolution of the wall flow pattern is almost the same at downstream of the cylinder. The wall flow pattern of the wake along the centerline is different each other. In case of thin *BL*, the width of the wake is spread to *Z*-direction. On the other hand, the wake is contracted to downstream, in case of thick *BL*.

Figure 6(b) presents the wall flow pattern, in case of $\theta = -10°$ *IFC*. At the upstream of the cylinder, both characteristic lines are observed almost the same tendency as the normal cylinder. At downstream of the cylinder, the larger size of convolution region of wall flow pattern is the same at both cases. The wider wake region is observed in this case, compared with normal cylinder. Also, the width of the wake is spread to *Z*-direction.

Figure 6(c) presents the wall flow pattern in case of $\theta = +10°$ *IBC*. The upstream characteristic lines both show the same tendency as other cases. The smaller size of convolution is observed. The approaching flow at higher spanwise location is turned around the cylinder and penetrates into the wake. The existence of twin type of Karman vortex is reported by Shizawa et al. (1998). The wake is spread to *Z*-direction just downstream of the cylinder and wider wake region is observed at thick *BL*.

Spectrum Analysis

Figure 7 to Figure 9 present the results of spectrum analysis by the normal hot-wire anemometer. Figure (a) presents the frequency spectrum $f\phi_{uu}$ distribution at several spanwise location of the cylinder. The symbol f is the frequency and ϕ_{uu} is the spectrum density of streamwise turbulence intensity. The $f\phi_{uu}$ shows constant value when the slope of ϕ_{uu} is 1, which corresponds to energy containing sub-range. The measurements are conducted at $X/D = 3$. The location corresponds to the formation region of Karman vortex by Gerrard (1996). Figure (b) is the spanwise change of peak value of Karman shedding frequency (*ksf*) and energy containing sub-range (*ecsr*). Two cases of inclined cylinder, inclined angle of ±10° are compared with normal cylinder.

Figure 7(a) presents the $f\phi_{uu}$ profile, in case of normal cylinder. At thin *BL*, the weak primary peak, which corresponds to *ksf*, is observed in the *BL*. The peak is observed almost the same value as other

cases at outside of the *BL*. At thick *BL*, the primary peak is clearly observed at each location. The characteristic of this case is that the harmonics of the primary peak is observed at thick *BL*. The wide frequency range of *ecsr* is shown at thin BL. Figure 7(b) presents the spanwise profile of peak value of *ksf* and *ecsr*. In the *BL*, the peak level of *ksf* at thin *BL* is almost twice of thick *BL* case. The differences are observed up to about $Y/\delta = 3$. On the other hand, the peak value of *ecsr* is the same except about $Y/\delta < 0.7$. The spanwise change of *ksf* is almost the same as *IFC* at thin *BL*, and is the same as *IBC* at thick *BL*. At thick *BL*, the near wall momentum of the flow is small, the weaker Karman vortex is enough to supply the extra momentum into the wake.

Figure 8 shows the spectrum $f\phi_{uu}$ distribution in case of $\theta = -10°$ *IFC*. Both figures present the same profile independent of the *BL* thickness. The only difference is the characteristic of the peak value of harmonics of *ksf*. The spanwise change of the value is almost the same in this case, as shown in Figure 8(b). This means that the structure of the wake is not depended on the *BL* thickness.

Figure 9(a) presents the $f\phi_{uu}$ profile, in case of *IBC*. Both the primary frequency of the *ksf* and its harmonics are hardly observed in this case. The level of *ecsr* is low and the frequency range is extremely wide at $Y/\delta = 0.4$. Figure 9(b) shows the spanwise profile of each peak. The peak of *ksf* is not observed at $Y/\delta < 0.4$. The characteristic of peak profile is the following. Both peaks show high values at thick *BL*. At thin *BL*, the flow with higher momentum turns around the cylinder and penetrates far into the *BL* compared with thick *BL* case. Then, it is no use to transport extra momentum in the wake by the Karman vortex. The effect is observed up to $Y/\delta > 3$.

CONCLUSIONS

The conclusions of the research are the followings.

1. The size of horseshoe vortex is changed exponentially with the change of inclined angle.
2. The rapid recovery is observed at downstream of the cylinder, in case of thick boundary layer.
3. The remarkable effects of boundary layer thickness on the structure of the wake are observed in case of normal cylinder. The structure is the same as inclined forward cylinder at thin boundary layer and is the same as inclined backward cylinder at thick boundary layer.
4. In case of small angle of inclined forward cylinder, the structure of the wake is not affected by the boundary layer thickness.
5. In case of small angle of inclined backward cylinder, the primary frequency of Karman vortex is not observed close to the wall.

REFERENCES

Bearman, P.W., 1969, "On Vortex Shedding from a Circular Cylinder in the Critical Reynolds Number Regime", J. fluid Mech., 37 – 3, 577 – 585.

Cimbala, J.M., Nagib, H.M. and Roshko, A., 1988, "Large Structure in the Far Wakes of Two-Dimensional Bluff Bodies", J. Fluid Mech., 190, 265 – 298.

Eckerle, W.A. and Langston, L.S., 1987, "Horseshoe Vortex Formation Around aCylinder", Trans. ASME, J. Turbomachinery, 109, 278 – 285.

Eckerle, W. A. and Awad, J. K., 1991, "Effect of Freestream Velocity on the Three-Dimensional Separated Flow region in Front of a Cylinder", Trans. ASME, J. Fluids Engineering, 113, 37 – 44.

Eibeck, P.A., 1990, "An Experimental Study of the Flow Downstream of a Circular and Tapered Cylinder", Trans. ASME, J. of Fluids Engineering, 112, 393 – 401.

Gerich, D. and Eckelmann, H., 1982, "Influence of End Plates and Free Ends on the Shedding Frequency of Circular Cylinders", J. Fluid Mech., 122, 109 – 121.

Gerrard, J.H., 1966, "The Mechanics of the Formation Region of Vortices behind Bluff Bodies", J. Fluid Mech. 25 – 2, 401 – 413.

Hanson, A. R., 1966, "Vortex Shedding from Yawed Cylinder", AIAA J., 4 – 5, 738 – 740.

Humphreys, J.S., 1960, "On a Circular Cylinder in a Steady Wind at Transition Reynolds Number", J. Fluid Mech., 9 – 4, 603 – 612.

Kline, S. J. and Mclintock, F. A., 1953, "Describing Uncertainties in Single-Sample Experiments", Mech. Engineering, 75, 3 – 8.

Mangalam, S. M., Venkateswaran, S. and Korategere, S., 1994, "Measurement of Surface flow Features at the Stagnation region of a Swept Cylinder", AIAA Paper, AIAA 94–0731.

Ramberg, S. E., 1983, "The Effects of Yaw and Finite Length upon the Vortex Wakes of Stationary and Vibrating Circular Cylinders", J. Fluid Mech., 128, 81 – 107.

Shizawa, T., Honami, S. and Miyauchi, K. 1998, "Near Wall Vortex Structures in an Inclined Cylinder Wake", AIAA Paper 98 – 0441.

Smith, R.A., et al. (1972), "Experimentas on Flow about a Yawed Ciercular Cylinder", Trans. ASME, J. Basic Enginnering, 771 – 776.

Stansby, P.K., 1974, "The Effects of End Plates on the Base Pressure Coefficient of a Circular Cylinder", Aero. J., 36 – 37.

Van Atta, C. W., 1968, "Experiments on Vortex Shedding from Yawed Circular Cylinders" AIAA J., 6 - 5, 931 – 933.

Williamson, C. H. K., 1989, "Oblique and Parallel Modes of Vortex Shedding in the Wake of a Circular Cylinder at Low Reynolds Numbers", J. Fluid Mech., 206, 579 – 627.

	δ mm	δ_2 mm	D/δ_2	Re_D	$Re_{\delta 2}$
Thin *BL*	18.1	1.92	15.6	2.5 x 10^4	1610
Thick *BL*	38.5	3.96	7.6	2.5 x 10^4	3990

Table 1 : Boundary layer parameters.

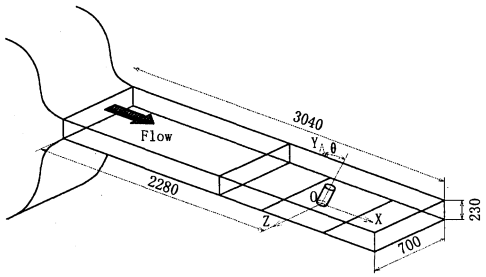

Fig 1 : Experimental set up (dimensions in mm).

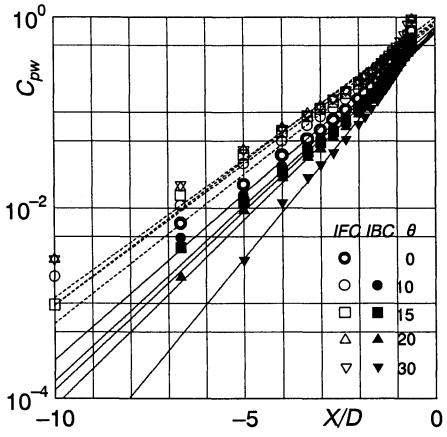

(a) : Thin boundary layer.

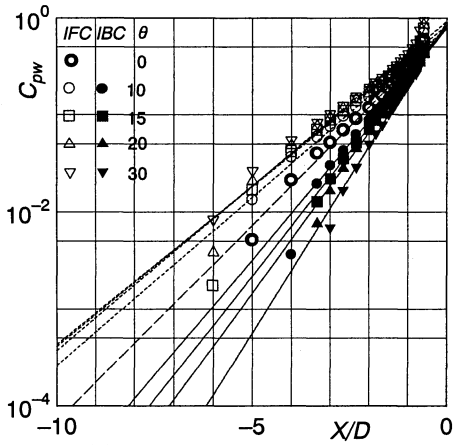

(b) : Thick boundary layer.

Fig 2 : C_{pw} profile (Upstream).

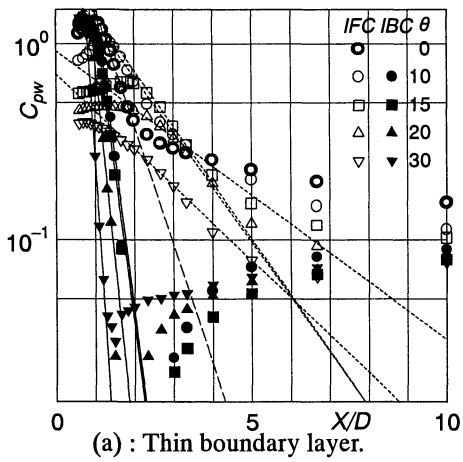

(a) : Thin boundary layer.

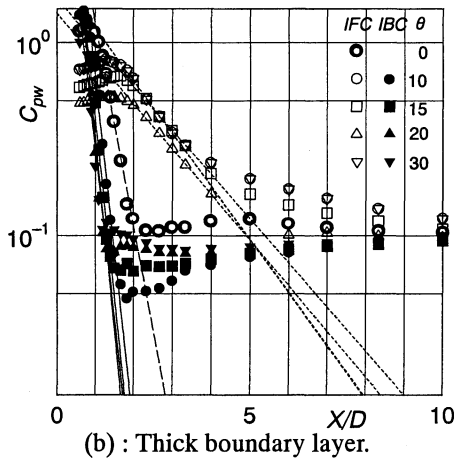

(b) : Thick boundary layer.

Fig 3 : C_{pw} profile (Downstream).

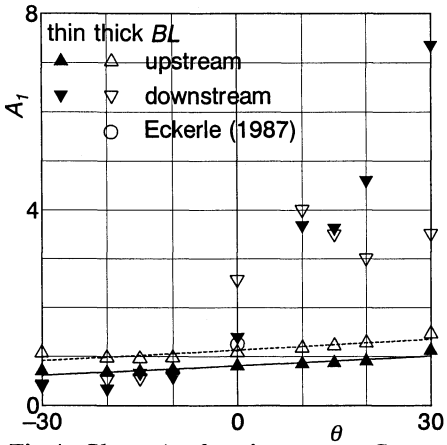

Fig 4 : Slope A_1 of static pressure C_{pw}.

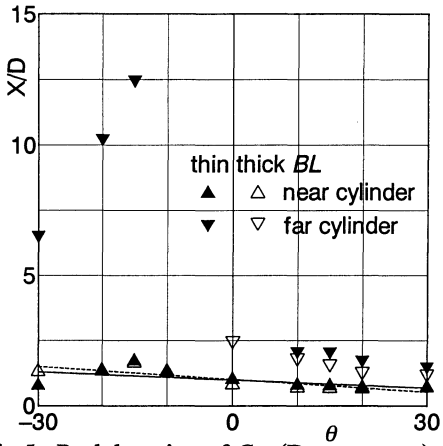

Fig 5 : Peak location of C_{pw} (Downstream).

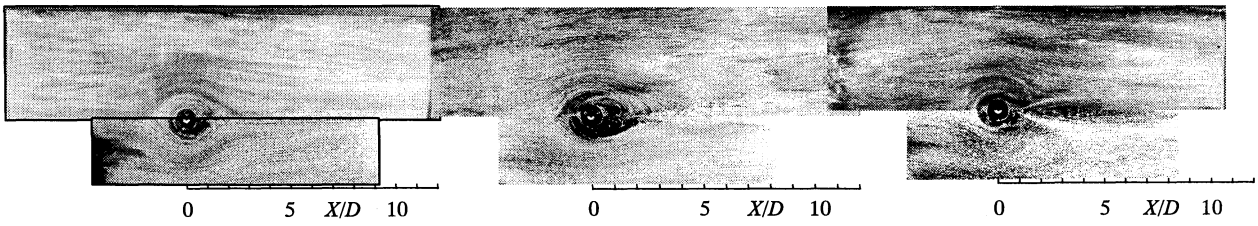

(a) Normal cylinder. (b) $\theta = -10°$ *IFC*. (c) $\theta = +10°$ *IBC*.

Fig 6 : Wall flow pattern (upper : Thin *BL*, lower : Thick *BL*).

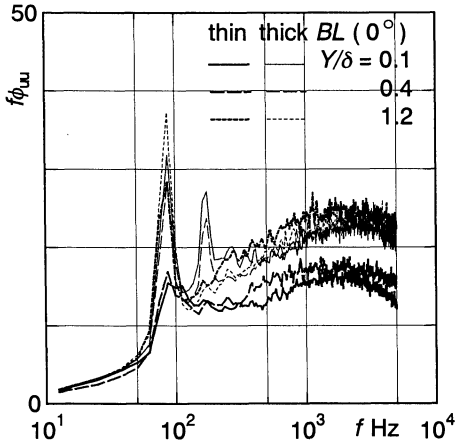

(a) Spectrum $f\phi_{uu}$ distribution.

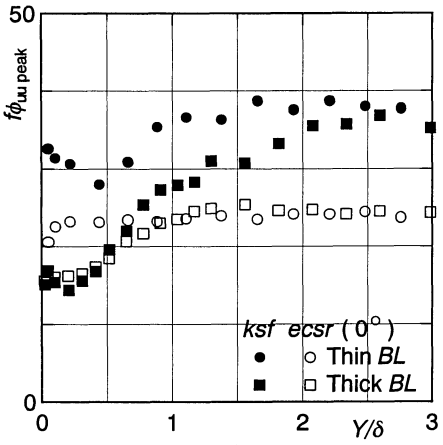

(b) Peak value of *ksf* and *ecsr*.

Fig 7 : Spectrum $f\phi_{uu}$ of Normal cylinder at $X/D = 3$.

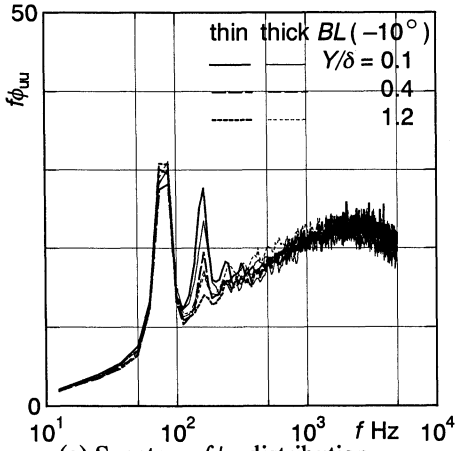

(a) Spectrum $f\phi_{uu}$ distribution.

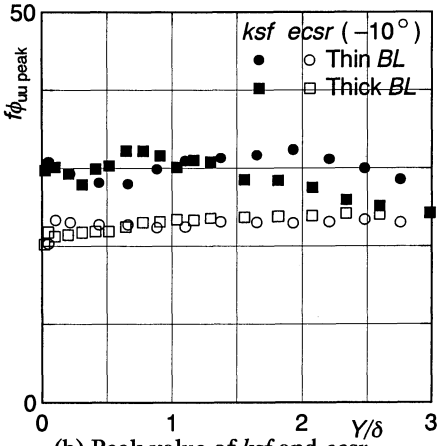

(b) Peak value of *ksf* and *ecsr*.

Fig 8 : Spectrum $f\phi_{uu}$ of $\theta = -10°$ *IFC* at $X/D = 3$.

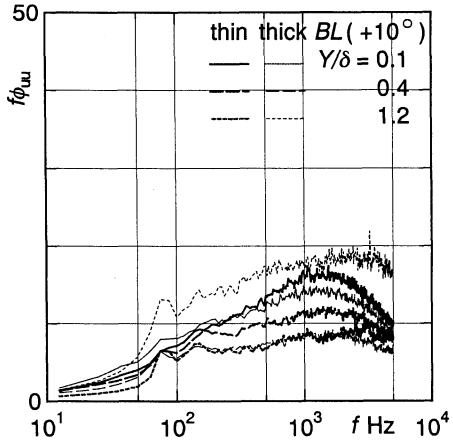

(a) Spectrum $f\phi_{uu}$ distribution.

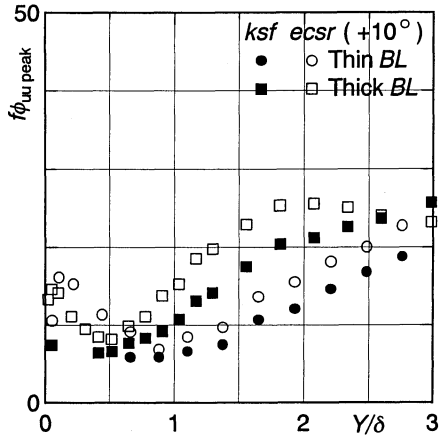

(b) Peak value of *ksf* and *ecsr*.

Fig 9 : Spectrum $f\phi_{uu}$ of $\theta = +10°$ *IBC* at $X/D = 3$.